Optical and structural properties of implanted Si wafers: the effects of implantation energy and subsequent isochronal annealing temperature

2006 Semicond. Sci. Technol. 21 1059

(http://iopscience.iop.org/0268-1242/21/8/013)

INSTITUTE OF PHYSICS PUBLISHING SEMICONDUCTOR SCIENCE AND TECHNOLOGY

Semicond. Sci. Technol. **21** (2006) 1059–1063 doi:10.1088/0268-1242/21/8/013

Optical and structural properties of implanted Si wafers: the effects of implantation energy and subsequent isochronal annealing temperature

Emmanouil Lioudakis, Constantinos Christofides and Andreas Othonos

Photonics and Optoelectronics Research Laboratory, Department of Physics, University of Cyprus, PO Box 20537, 1678, Nicosia, Cyprus

E-mail: mlioud@ucy.ac.cy

Received 20 March 2006, in final form 15 May 2006
Published 28 June 2006
Online at stacks.iop.org/SST/21/1059

Abstract

We have studied the influence of implantation energy and subsequent isochronal annealing temperature on the optical and structural properties of implanted Si wafers employing a multiwavelength spectroscopic ellipsometer. A temperature-dependent multilayer optical model is used to explain the ellipsometric data for all implantation energies (20 to 180 keV) and annealing temperatures (300 to 1100 °C) of this work. This work completely characterizes the structural and optical properties of these implanted samples via the pseudodielectric functions and the integrated damage depth profile. For the highest implantation sample self-annealing phenomena have appeared, reducing the integrated damage depth profile. Finally, the dynamics of isochronal annealing temperature on the integrated damage depth profile of these wafers exhibit an abrupt drop in the transition temperature where a long-range ordering is obtained and pseudodielectric functions approach the crystallinity shapes.

1. Introduction

It is well known that ion implantation is a key technological process in modern microelectronics and is introduced as an alternative to diffusion for the semiconductor doping process. One of the main disadvantages of the ion implantation process is the damage caused to the material resulting from the energetic character of the progress [1]. The consequence of ion implantation is the amorphization of the semiconductor wafer and the presence of electrical defects. Ion implantation, therefore, must be followed by an annealing process for the semiconductor to recover its crystallinity and for the doping impurities to become electrically active. Over the last four decades the importance of ion implantation as an alternative technique for semiconducting doping has led to a development of many characterization techniques.

Spectroscopic ellipsometry is an easy, non-destructive technique [2] for detecting and characterizing the degree of crystallinity in buried layers, in addition to the depth profiling of the sample [3]. Recently, the optical properties of implanted Si wafers [4, 5], and the redistribution of the impurity atoms (vacancies, interstitial pairs, etc . . .) as well as the annihilation of the damaged material due to the rapid thermal annealing have also been studied [6]. The use of ellipsometry may allow the study of the redistribution of the impurity atoms and the annihilation of the damaged material due to the isochronal thermal annealing [7]. This annealing process is completely different from previous processes (rapid annealing) as the temperature plays a crucial role in the dynamics of optical and structural properties of materials. In this work, we present a comprehensive optical study on implanted silicon wafers with spectroscopic ellipsometry in the photon-energy range of 1.5–6 eV. This study adds further information in clearly

understanding the structural and optical properties of this material.

2. Experimental details

It is known that the influence of implantation dose and energy as well as the subsequent annealing in the structural properties of silicon wafers reveals changes in the electronic energy-band structure and, therefore, in the optical properties of this material. The samples used in this work are crystalline silicon wafers implanted at different energies (20 to 180 keV) with constant implantation dose 5×10^{14} P^+ cm^{-2}. The phosphorous implantation was performed through a thin oxide layer (∼2 nm) at room temperature. Some of the samples were then annealed isochronally at various temperatures ranging from 300 to 1100 °C for 1h in an inert nitrogen atmosphere. A multilayer optical model that takes into account the density of ion-induced vacancies is developed to analyse the spectroscopic ellipsometry response (i.e. $\tan\Psi$ and $\cos\Delta$, where Ψ and Δ are ellipsometric angles). The Bruggeman effective medium approximation (BEMA) [8, 9] combined with Monte Carlo simulations of penetration of phosphorus ions in silicon [10] have been used to determine the dielectric functions for all wafers under investigation in this work. In this model the calculated damage depth (from TRIM software) for each wafer d_T is divided into $m = 5$ sublayers with equal thickness $z_m = d_T/m$. Each sublayer has its own complex dielectric function. The damage level of each wafer is calculated using an upgraded damage depth profile function [11].

$$D(z_m, E, T) = 1 - \exp[-f(E, T) \times \exp[-(z_m - \mu(E, \mathrm{T}))^2/2\sigma^2(E, T)],$$

where $f(E, T)$ is the fraction of amorphous phase (a-Si) which depends on the implantation energy, $\mu(E, T)$ and $\sigma(E, T)$ are respectively the estimated mean value and standard deviation of the density of ion-induced vacancies from TRIM calculations. We should point out that the parameters f, μ, σ of our model are dependent on the annealing temperature and, the density of ion-induced vacancies refers to vacancy–interstitial pairs (Frenkel pairs) [12]. It is known that the amorphization in crystalline silicon is much more complex than simply vacancy formation. It entails formation of Frenkel pairs, point defects and amorphous nanoclusters [13] where collision cascades are located.

3. Results and discussion

In what follows we will present the pseudodielectric functions allowing us to extract structural and optical properties of the material. Initially, we make use of Monte Carlo simulations for the ion implantation which provide a structural depth profile model for the samples under investigation. This multilayer model is utilized in a reconstruction program fitting to the associated ellipsometric data to obtain the fraction of amorphous phase for each layer. Finally, we calculate the integrated damage depth profile as a function of annealing temperature in order to determine the transition temperature.

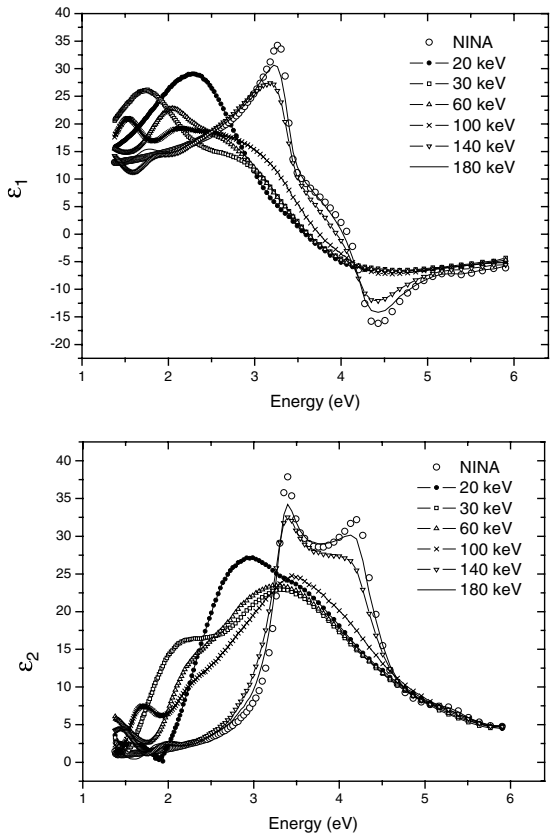

Figure 1. Pseudodielectric functions of Si wafers at different implantation energies (20 to 180 keV), with a constant implantation dose of 5×10^{14} P^+ cm^{-2}. The open circles show the non-implanted and non-annealed reference sample for comparison purposes.

The changes to pseudodielectric functions for different implantation conditions reflect the structural changes to the material due to the induced damage. These changes modify the band structure of the material, which in turn modify the optical properties of the material. Figure 1 shows the pseudodielectric functions of non-annealed silicon wafers for different implantation energies. These curves give a complete characterization of the optical properties of the material, indicating the critical points (peaks of imaginary parts of the dielectric function), the critical implantation energy (when the structure achieves long-range ordering) and the amorphization profile of the structure (the induced damage depth profile). Increasing the implantation energy the bombarded phosphorous ions penetrate further into the silicon target, causing greater overall amorphization. This is provided from the generated inner-boundaries inside the silicon target at different depths from the surface, which cause oscillations in the pseudodielectric functions of the material at low energies.

As seen from figure 1, by changing the implantation energy the pseudodielectric functions are significantly altered. As a result the optical properties of these implantation samples appear to have a complex behaviour [9]. It is interesting to point out that even for the sample with the lower implantation energy 20 keV, the ion-induced damage is apparent where the dielectric functions approach the spectral shape of amorphous silicon. With increasing implantation energy the critical points

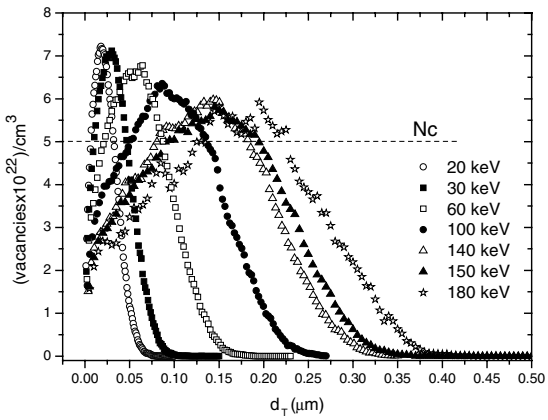

Figure 2. Reconstruction of the amorphization profile using Monte Carlo simulations of the phosphorus ion implantation in silicon at various implantation energies. The horizontal line represented by Nc corresponds to the critical amorphization density.

move to higher energies. At 100 keV the pseudodielectric functions approach those associated for crystals where three critical points (exactly as in the crystalline silicon) appear [14]. This value is known as critical implantation energy (100 keV) at which point the material is believed to maintain its periodic structure.

We should point out that these results coincide with the Monte Carlo calculations at various implantation energies and constant doping concentration 5×10^{14} P^+ cm^{-2} (figure 2).

We note that for all wafers implanted at different energies the density of ion-induced vacancies is higher than the critical amorphization density ($N_c = 5 \times 10^{22}$ cm^{-3}) and gradually decreases when increasing the implantation energy. As seen from figure 2 the mean value of the ion-induced damage profile is shifted to higher values and the standard deviation is broadened when increasing the implantation energy. Furthermore, the fraction of amorphous phase gradually decreases when increasing the implantation energy.

Although the pseudodielectric functions reflect the structural changes of the Si wafers, this ion-induced damage can be reversed by thermal isochronal annealing [7]. In figure 3 we show the temperature evolution of pseudodielectric functions for a wafer with 5×10^{14} P^+ cm^{-2} and 20 keV. The optical properties of this sample change gradually due to the annealing temperature ranging from 300 to 1100 °C. With increasing annealing temperature the peaks of the transition energies are moved to higher energies approaching those of the non-implanted, non-annealed Si reference sample (points). We note that this wafer appears to have a phase transition between 700 and 800 °C without oscillations for low energies. Above this temperature the pseudodielectric functions exhibit an abrupt long-range ordering due to the recovery of lattice periodicity indicated by the three critical points [14].

For the highest implanted wafer (180 keV) and for the same beam current density, the pseudodielectric functions exhibit a different spectra behaviour (figure 4) compared with the other implanted samples. Under these implantation conditions the lattice periodicity remains intact, and thus the subsequent isochronal annealing affects the pseudodielectric functions only in the vicinity of critical points. From these

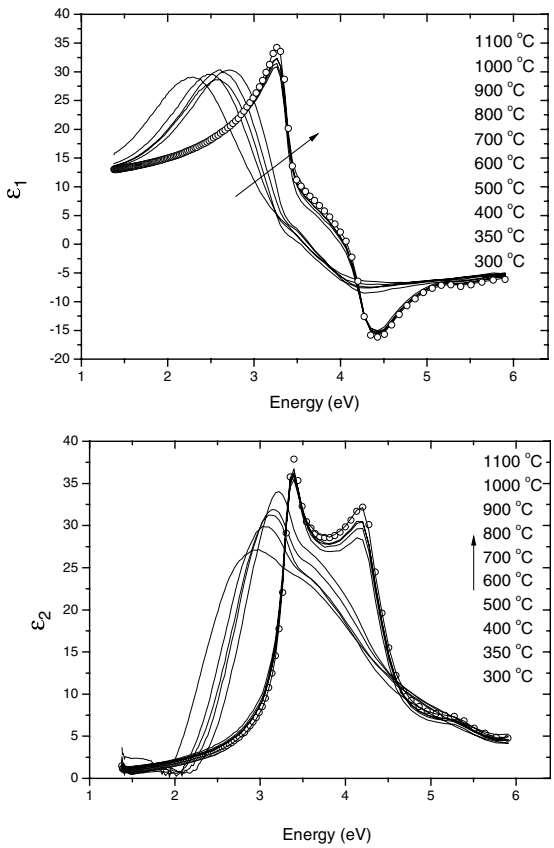

Figure 3. Evolution of pseudodielectric functions of the Si wafer with 5×10^{14} P^+ cm^{-2} and 20 keV at various annealing temperatures ranging from 300 to 1100 °C. The open circles show the non-implanted and non-annealed reference sample for comparison purposes.

results, we should point out that the isochronal annealing temperature has a slight effect on the structural changes of wafers, modifying the electronic band structure of the material. We should point out that we have studied the effects of subsequent isochronal annealing temperature for all implantation samples under investigation in this work using our multilayer model.

The fitting process utilized in this work is the nonlinear Levenberg–Marquardt regression method and the error function is defined by the formula

$$\chi = \left\{ \frac{1}{(N-P-1)} \sum_{j=1}^{N} \left[\left(\cos \Delta_j^{\text{meas}} - \cos \Delta_j^{\text{regr}} \right)^2 + \left(\tan \Psi_j^{\text{meas}} - \tan \Psi_j^{\text{regr}} \right)^2 \right] \right\}^{1/2},$$

where N represents the number of independently measured values corresponding to different wavelengths and P the number of unknown model parameters. (Here 'meas' and 'regr' refer to measured and regression values, respectively).

Due to the gradual recrystallization of the wafers (due to the annealing), either damaged regions were eliminated ($D(z_m) = 0$) or the concentration of amorphous to crystalline silicon in the mixture layers was decreased and consequently

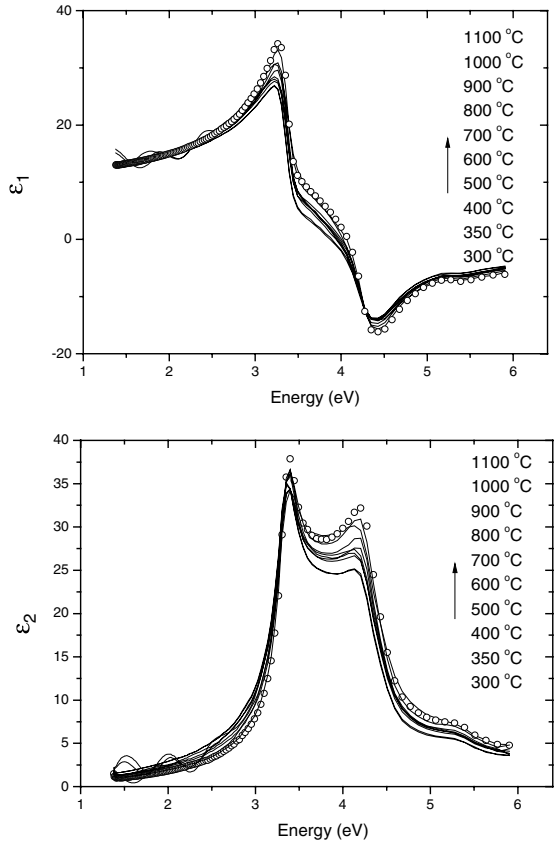

Figure 4. Evolution of pseudodielectric functions of an Si wafer with 5×10^{14} P^+ cm^{-2} and 180 keV at various annealing temperatures ranging from 300 to 1100 °C. The open circles show the non-implanted and non-annealed reference sample for comparison purposes.

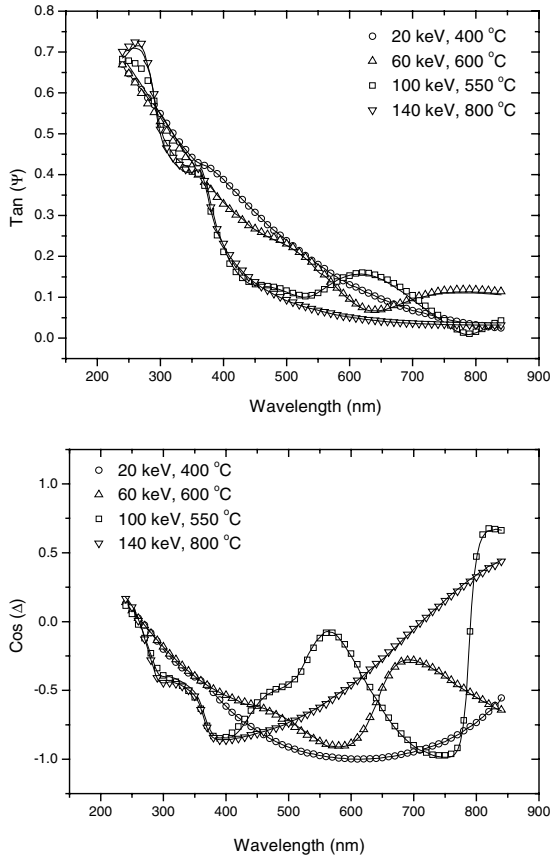

Figure 5. Fitting curves (solid lines) throughout the experimental ellipsometric data (points) using the above analysis for various wafers at different implantation energies and annealing temperatures.

the mixture layers were replaced by the crystalline silicon. Some typical fitting curves on ellipsometric parameters ($\tan\Psi$ and $\cos\Delta$) for implanted Si wafers are presented in figure 5. As seen from these results, our multilayer model describes well all implanted samples (20 to 180 keV) upon the isochronal annealing temperature.

Based on the above ellipsometric analysis we should point out that the integrated damage depth profile function of our multilayer model $I(E,T) = \int_0^{d_T} D(z,E,T)\,\mathrm{d}z$ exhibits an abrupt drop for all implanted wafers for (600–700 °C), depicting the generality of the transition temperature (see figure 6) in these samples. The only noticeable change is the recrystallization temperature of the highest implantation energy (500–600 °C). We believe that in this highest implantation some annihilation mechanisms lead to self-annealing of the lattice damage from the heat generated during ion implantation [15]. This is attributed to the high kinetic energy of the implanted ions resulting in a sufficient rise of temperature on the surface in comparison to the lower implantation samples. At this point we should emphasize that self-annealing has been confirmed in similar samples under the same experimental conditions [16]. Finally, we note that due to the change of ion damaged depth d_T by the implantation, the spatial resolution of our model changes. Consequently, the accuracy of our model depends on the number of sublayers, which increases the computation time.

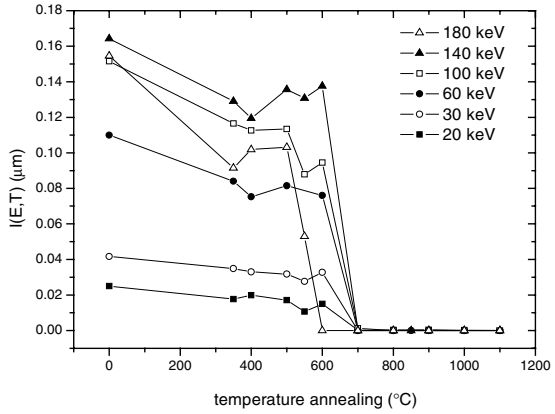

Figure 6. Dynamic of isochronal annealing temperature on the damage depth profile for all implantation energies under investigation in this work.

4. Conclusions

In this work we have presented the evolution of optical properties (pseudodielectric functions) for implanted non-annealed and isochronal annealed silicon wafers. The

implantation conditions vary from 20 to 180 keV at an implantation dose of 5×10^{14} P^+ cm^{-2}. The pseudodielectric functions for all these implantation samples reveal structural changes as a result of implantation as well as the recovery of a long-range periodic order with the subsequent isochronal annealing. Based on a temperature-dependent multilayer structural model we have investigated the temperature evolution of the structural properties of implanted silicon wafers, extracting crucial parameters such as amorphization profile, critical points and critical implantation energy. Furthermore, we have observed a drop in the integrated damage depth profile at the highest implant (180 keV), which is believed to be due to the self-annealing effect under these experimental conditions. It should be noted that the implantation energy and isochronal annealing temperature are key contributing factors to the structural changes of the material and consequently to its optical properties.

References

[1] Benton J L, Libertino S, Kringhoj P, Eaglesham D J, Poate M and Coffa S 1997 *J. Appl. Phys.* **82** 120

[2] Lioudakis E and Othonos A 2005 *Opt. Eng.* **44** 023802

[3] Mori H, Adachi S and Takahashi M 2001 *J. Appl. Phys.* **90** 87

[4] Kurihara K, Hikino S and Adachi S 2004 *J. Appl. Phys.* **96** 3247

[5] Tsunoda K, Adachi S and Takahashi M 2002 *J. Appl. Phys.* **91** 2936

[6] Hikino S and Adachi S 2004 *J. Phys. D: Appl. Phys.* **37** 1617

[7] Lioudakis E, Cristofides C and Othonos A 2006 *J. Appl. Phys.* at press

[8] Aspnes D E 1981 *Thin Solid Films* **81** 249

[9] Lioudakis E, Nassiopoulou A G and Othonos A 2006 *Thin Solid Films* **496** 253

[10] Ziegler J F, Biersack J P and Littmark U 1985 *The Stopping Range of Ions in Solids* (Tarrytown, NY: Pergamon)
Ziegler J F and Biersack J P 2003 TRIM software, SRIM-version 2003.26 (http://www.srim.org/)

[11] Fried M, Lohner T, Aarnink W A M, Hanekamp L J and van Silfhout A 1992 *J. Appl. Phys.* **71** 2835

[12] Weber W J 2000 *Nucl. Instrum. Methods Phys. Res.* B **166–167** 98

[13] Weber W J, Gao F, Devanathan R, Jiang W and Wang C M 2004 *Nucl. Instrum. Methods Phys. Res.* B **216** 25

[14] Hull R 1999 *Properties of Crystalline Silicon INSPEC* (London, UK: The Institution of Electrical Engineers)

[15] Othonos A and Christofides C 2002 *Phys. Rev.* B **66** 085206

[16] Seas A and Christofides C 1995 *Appl. Phys. Lett.* **66** 3346